Japanese Journal of Comprehensive Rehabilitation Science (2025)

Original Article

Real-Time Estimation of Lower Limb Posture and Joint Angles Using Wearable IMUs: Reproduced Hemiparetic and Normal Gait

Shun Kanega, Master's degree,[1,2] Yoshihiro Muraoka, PhD[1,2]

[1]Faculty of Human Sciences, Waseda University, Tokorozawa, Saitama, Japan
[2]National Hospital Organization Murayama Medical Center, Musashimurayama, Tokyo, Japan

ABSTRACT

Kanega S, Muraoka Y. Real-Time Estimation of Lower Limb Posture and Joint Angles Using Wearable IMUs: Reproduced Hemiparetic and Normal Gait. Jpn J Compr Rehabil Sci 2025; 16: 19–29.

Objective: A low-computational-load posture estimation method was employed, assuming integration into a functional electrical stimulation (FES) device, to estimate thigh and shank inclination angles as well as the knee joint angle during gait. The accuracy and processing time of the method were evaluated to assess its practical feasibility.

Methods: Two inertial measurement units (IMUs) were mounted on the lateral thigh and shank. Two healthy adults performed level-ground gait, including normal gait and gait reproducing the characteristics of circumduction gait, which is typically observed in individuals with post-stroke hemiparesis. A custom gait pacemaker was developed to replicate the spatiotemporal asymmetry of hemiparetic gait. Posture estimation in the sagittal and frontal planes was performed on a microcontroller using a low-computational-load Madgwick filter, and the processing time was recorded. The estimation accuracy was assessed by comparing the results with optical motion capture data using root mean square error (RMSE) and cross-correlation analysis.

Results: The average total processing time, including sampling, posture estimation, and stimulation control, was 6.8 ms. The RMSE of sagittal plane posture angles was less than 4° in all cases, suggesting estimation accuracy comparable to previous studies. For the frontal plane posture angles, the estimation accuracy was relatively high during the reproduced circumduction gait, indicating that the system effectively captured the circumduction motion. Conversely, the accuracy tended to be lower during normal gait.

Conclusion: Compared with previous studies, the posture estimation method used in this study, which employed the Madgwick filter, was able to estimate posture without compromising accuracy. The entire process, including sampling, posture estimation, and stimulation control, was completed within 10 ms, reflecting the feasibility of real-time processing at 100 Hz.

Key words: 6-axis IMU, circumduction gait, thigh inclination angle, shank inclination angle, knee joint angle

Correspondence: Yoshihiro Muraoka, PhD
Faculty of Human Sciences, Waseda University, 2−579−15, Mikajima, Tokorozawa, Saitama 359−1192, Japan.
E-mail: y.muraoka@waseda.jp

Accepted: April 9, 2025.
Conflict of Interest Statement: The authors declare that there are no conflicts of interest regarding the publication of this paper.

Introduction

1. Post-Stroke Hemiplegic Gait and Functional Electrical Stimulation

In stroke patients with hemiplegia, gait is often characterized by a significant loss of symmetry and coordination, leading to the adoption of compensatory strategies. For example, when foot clearance is reduced, the paretic limb may swing outward during circumduction gait to prevent tripping. During the rehabilitation process, regularly assessing gait patterns and joint range of motion using parameters, such as lower-limb posture angles and joint angles, is essential. These posture-related parameters can also be used to control functional electrical stimulation (FES). FES is a therapeutic approach that compensates for the impaired motor function caused by stroke or spinal cord injury by electrically stimulating the paralyzed muscles [1−3]. It has been reported to improve forward

propulsion and limb swing in the paretic leg during gait [1]. Real-time identification of the gait phase is necessary to apply FES during movement. Conventional methods employ foot switches [4], tilt sensors [5], and, more recently, rule-based control using inertial measurement units (IMUs) [6–9]. However, the abnormal gait in stroke patients with hemiplegia often involves atypical and highly variable limb alignments due to factors such as spasticity and contracture. Consequently, methods developed for healthy individuals may fail to accurately detect gait phases in these populations [8, 9]. Therefore, incorporating posture information into gait phase estimation and stimulus timing is necessary. Currently, most FES systems are designed specifically for foot drop [5], typically identifying the swing phase to apply electrical stimulation to the tibialis anterior muscle. However, gait abnormalities are not limited to the swing phase. Abnormal lower-limb alignment, such as knee buckling or genu recurvatum, can occur during the stance phase. Thus, posture estimation and FES throughout the gait cycle are considered beneficial. Furthermore, IMUs enable simultaneous gait assessment in daily living environments with the ability to transmit and store data via cloud services. This feature is useful for post-discharge follow-up and orthosis selection during stroke gait rehabilitation. Therefore, this study aimed to evaluate the accuracy of posture estimation, which is a fundamental component of gait phase detection and FES control during abnormal gait.

2. Quantitative Posture Measurement

High-precision optical motion-capture systems have traditionally been used for quantitative posture measurements during gait. However, owing to limitations, such as high equipment costs and the time required to mount reflective markers, their use is constrained by the measurement environment. Posture estimation using IMUs has become increasingly common [10–17]. IMUs offer several advantages, including low cost, compact size, high portability, and fewer environmental constraints. Nonetheless, IMUs exhibit certain limitations. Accelerometers measure linear acceleration and estimate orientation angles from the direction of gravity under static conditions. However, during movement, additional acceleration components interfere, reducing estimation accuracy. Conversely, gyroscopes measure angular velocity and can estimate orientation by integrating these values over time; however, this integration leads to cumulative drift errors. To overcome these limitations, various sensor-fusion methods have been developed, including Kalman filters [12], nonlinear Kalman filters adapted for nonlinear systems [13, 14], complementary filters [15, 16], and Madgwick filters [17].

3. Advantages of Madgwick Filter

Among the aforementioned sensor fusion methods, posture estimation using nonlinear Kalman filters, which offer high estimation accuracy, is commonly employed. However, owing to their high computational load, processing time becomes an issue when implementing them on low-power, low-performance hardware, such as microcontrollers. Moreover, when posture estimation is incorporated into an FES device, posture estimation and electrical stimulation control must be performed using a microcontroller, which necessitates a less computationally intensive estimation method. Conversely, the Madgwick filter, which is a type of complementary filter, provides comparable accuracy to conventional Kalman filters while significantly reducing processing time [17]. Feng et al. (2017) compared the processing times of the Madgwick filter and various Kalman filters and reported that the Madgwick filter was substantially faster [18]. Although the Madgwick filter is known to produce less accurate estimates than nonlinear Kalman filters in complex movements, such as sports actions or running, which involve large translational accelerations, it may offer comparable accuracy in relatively simple and slow movements such as gait. If processing can be completed in a sufficiently short time, the Madgwick filter may be applicable to FES control. Additionally, the Madgwick filter has been used in applications such as joint angle estimation during treadmill gait [19] and orientation tracking of canes [20]; however, its posture estimation accuracy in post-stroke hemiplegic gait has not yet been sufficiently validated.

Therefore, this study aimed to evaluate the accuracy of posture estimation using a low-computational-load Madgwick filter under gait conditions by applying FES in stroke patients with hemiplegia. Most previous studies using nonlinear Kalman filters performed computations on a PC; conversely, this study assumed the integration of the estimation algorithm into an FES device. Accordingly, posture estimation was executed using a microcontroller, and the processing time was recorded. Additionally, to accurately reproduce the spatiotemporal asymmetry typical of post-stroke hemiplegic gait and standardize gait conditions, a custom gait pacing device was developed and used. Healthy adults with clinical experience mimicked the hemiparetic gait during level-ground walking, and the lower-limb posture was estimated under these conditions. Finally, the estimated posture and joint angles were compared with reference data obtained from an optical motion capture system to evaluate estimation accuracy.

Methods

1. IMU-Based Posture Estimation Device

A knee-supporter-type posture estimation device was

developed by mounting IMUs on the thigh and shank. The IMU mounting positions are shown in Figure 1a. To facilitate easy mounting and removal of the IMUs, hook-and-loop fasteners (Velcro) were sewn onto the knee supporter, and the IMUs were fitted with corresponding fasteners to enable easy attachment and detachment. Two IMU modules (ICM-42688, TDK; dimensions: 12.8 × 10.2 × 3.0 mm; weight: approx. 3.0 g), capable of measuring three-axis acceleration and three-axis angular velocity, were used and mounted laterally on the thigh and shank, as shown in Figure 1a.

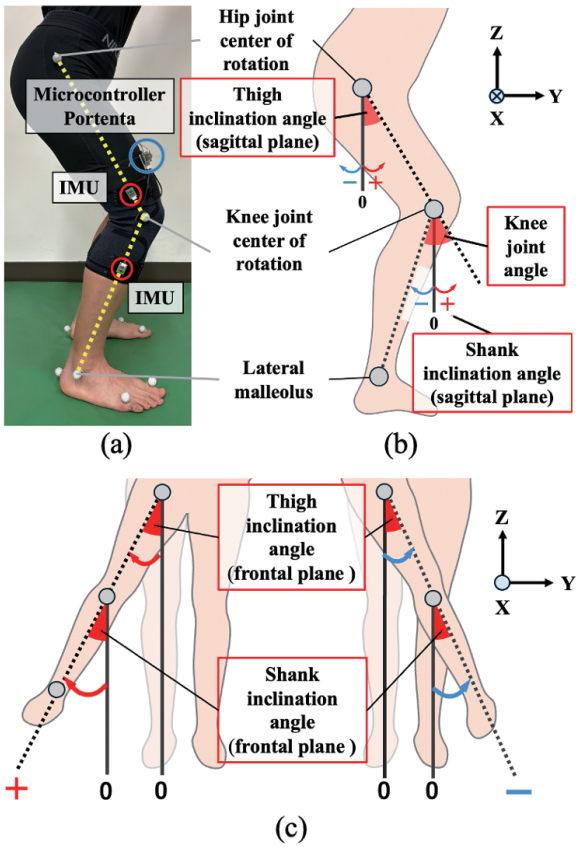

Figure 1. IMU mounting positions, and definition of posture angles and joint angles. (a) shows the IMU mounting position, (b) shows the sagittal plane orientation angle, and (c) shows the frontal plane orientation angle.

2. Analyzed Posture and Joint Angles and Coordinate Axes

In this study, the analyzed variables were the posture angles in the sagittal and frontal planes, as defined in Table 1. Figures 1b and 1c illustrate the analyzed posture and joint angles in the sagittal and frontal planes, respectively. The global coordinate system used in this study was defined as a right-handed system with the negative Z-axis aligned with the direction of gravity. The X-axis represents the anterior-posterior direction during gait, Y-axis medial-lateral, and Z-axis vertical. The rotation around the X-axis is defined as the roll angle (ϕ), Y-axis pitch angle (θ), and Z-axis yaw angle (ψ). The sagittal plane is defined as the plane perpendicular to the Y-axis and the frontal plane perpendicular to the X-axis. The knee joint angle is defined as the relative angle of the shank axis with respect to thigh axis. Because the knee joint can functionally be regarded as a hinge joint [21], only the sagittal plane was analyzed for the knee joint angle. Posture and joint angles in the sagittal plane are primarily used in FES control, whereas frontal plane posture angles were included in the analysis to capture circumductive movements.

3. Posture Estimation Using Madgwick Filter

Figure 2 shows a flowchart of the posture-estimation algorithm using the Madgwick filter. The Madgwick filter is a complementary filter used to mitigate gyroscope drift. Unlike conventional complementary filters, it employs a gradient descent algorithm. Additionally, the filter represents the orientation using a quaternion q, which consists of a scalar part (q_0) indicating the rotation angle and a vector part (q_1, q_2, q_3) indicating the rotation axis, as expressed by:

$$q = [q_0\ q_1\ q_2\ q_3] \quad (1)$$

There are two versions of the Madgwick filter: one that uses only an IMU and another that uses an IMU and a magnetometer [17]. In three-dimensional posture estimation, a magnetometer is required to correct the yaw angle drift. However, magnetometers are sensitive to interference from surrounding ferromagnetic materials [22, 23], which limits their accuracy in clinical and home environments. Therefore, following

Table 1. Definitions of posture and joint angles in the sagittal and frontal planes analyzed.

Analysis target	Definition of posture/Joint angles	Reference	Sign convention
Thigh inclination angle (sagittal plane)	Angle between the Z-axis and the thigh axis in the XZ plane	Z-axis (gravity direction): 0°	Backward tilt: +
Shank inclination angle (sagittal plane)	Angle between the Z-axis and the shank axis in the XZ plane	Z-axis (gravity direction): 0°	Backward tilt: +
Knee joint angle (sagittal plane)	(Thigh inclination angle in sagittal plane) − (Shank inclination angle in sagittal plane)	Knee extension: 0°	Flexion: +
Thigh inclination angle (frontal plane)	Angle between the Z-axis and the thigh axis in the YZ plane	Z-axis (gravity direction): 0°	Abduction: +
Shank inclination angle (frontal plane)	Angle between the Z-axis and the shank axis in the YZ plane	Z-axis (gravity direction): 0°	Abduction: +

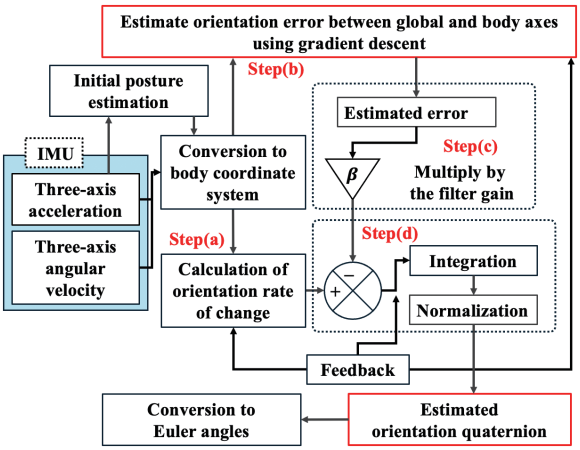

Figure 2. Flowchart of the posture angle estimation algorithm using the Madgwick filter.

previous research [24], a magnetometer was not used in this study, which focused on posture angles in the sagittal and frontal planes. Additionally, excluding the magnetometer reduced the computational load by less than half [17]. Accordingly, the Madgwick filter used in this study estimates the orientation of the IMU coordinate system relative to the global coordinate system in quaternion form, using 3-axis acceleration and angular velocity as inputs.

The posture estimation algorithm based on the Madgwick filter is outlined in four steps (a) to (d), as illustrated in Figure 2. In Step (a), the rate of change in orientation is calculated from the angular velocity. In Step (b), the orientation error between the global and body coordinate axes owing to rotation is estimated using a gradient descent method based on acceleration. In Step (c), the estimated error is scaled by the filter gain β. In this study, the filter gain β was set to 0.1. Finally, in Step (d), the orientation change rate obtained from the angular velocity is corrected using the scaled error and integrated over time to estimate the orientation quaternion.

The posture during quiet standing immediately before gait initiation was used as the initial posture for each trial. The initial posture (ϕ_0, θ_0, ψ_0) was calculated from the direction of gravity measured by the accelerometer, as shown in Equation (2), where a_x, a_y, and a_z are the outputs of the accelerometer along the three axes. Because the yaw angle (ψ) cannot be determined from acceleration data alone, it was set to $\psi_0 = 0$ as an initial condition. For simplicity, the vertical axis of the body coordinate system was assumed to align with the Z-axis of the global coordinate system [25–27]. Based on this assumption, the posture of the body coordinate system relative to the global coordinate system is estimated using Equation (3) (static calibration). Equation (3) represents the application of a rotation matrix R_0, computed from the initial posture (ϕ_0, θ_0, ψ_0), to the IMU output data S_{out}, which consists of three-axis acceleration (a_x, a_y, a_z) and three-axis angular velocity (g_x, g_y, g_z). During processing using the Madgwick filter, the orientation was represented using quaternions. To compare the orientation angles measured by the motion capture system, the resulting quaternions were converted into Euler angles (rotation order ZYX) using Equation (4). Additionally, Equation (5) enables conversion from Euler angles to quaternions.

$$\begin{bmatrix}\phi_0\\ \theta_0\\ \psi_0\end{bmatrix}=\begin{bmatrix}\arctan 2\,(a_y, a_z)\\ \arctan 2\,(-a_x, \sqrt{a_y^2+a_z^2})\\ 0\end{bmatrix} \tag{2}$$

$$R_0 S_{out}=\begin{bmatrix}\cos\theta_0 & 0 & -\sin\theta_0\\ \sin\phi_0\sin\theta_0 & \cos\phi_0 & \sin\phi\cos\theta_0\\ \cos\phi_0\sin\theta_0 & -\sin\phi_0 & \cos\phi\cos\theta_0\end{bmatrix}\begin{bmatrix}S_x\\ S_y\\ S_z\end{bmatrix} \tag{3}$$

$$\begin{bmatrix}\phi\\ \theta\\ \psi\end{bmatrix}=\begin{bmatrix}\arctan 2\left(2(q_0q_1+q_2q_3), 1-2(q_1^2+q_2^2)\right)\\ \arcsin\left(2(q_0q_2-q_1q_3)\right)\\ \arctan 2\left(2(q_1q_2+q_0q_3), 1-2(q_2^2+q_3^2)\right)\end{bmatrix} \tag{4}$$

$$\begin{bmatrix}q_0\\ q_1\\ q_2\\ q_3\end{bmatrix}=\begin{bmatrix}\cos\left(\frac{\phi}{2}\right)\cos\left(\frac{\theta}{2}\right)\cos\left(\frac{\psi}{2}\right)+\sin\left(\frac{\phi}{2}\right)\sin\left(\frac{\theta}{2}\right)\sin\left(\frac{\psi}{2}\right)\\ \sin\left(\frac{\phi}{2}\right)\cos\left(\frac{\theta}{2}\right)\cos\left(\frac{\psi}{2}\right)-\cos\left(\frac{\phi}{2}\right)\sin\left(\frac{\theta}{2}\right)\sin\left(\frac{\psi}{2}\right)\\ \cos\left(\frac{\phi}{2}\right)\sin\left(\frac{\theta}{2}\right)\cos\left(\frac{\psi}{2}\right)+\sin\left(\frac{\phi}{2}\right)\cos\left(\frac{\theta}{2}\right)\sin\left(\frac{\psi}{2}\right)\\ \cos\left(\frac{\phi}{2}\right)\cos\left(\frac{\theta}{2}\right)\sin\left(\frac{\psi}{2}\right)-\sin\left(\frac{\phi}{2}\right)\sin\left(\frac{\theta}{2}\right)\cos\left(\frac{\psi}{2}\right)\end{bmatrix} \tag{5}$$

4. Gait Conditions

The primary characteristics of a hemiparetic gait include reduced gait speed and increased gait asymmetry. In the present study, healthy adults reproduced the circumduction gait typically observed in stroke patients with hemiplegia, thereby performing a pseudo-circumduction gait. To ensure the reliability of the pseudo-circumduction gait, the participants were healthy individuals with clinical experience and a thorough understanding of poststroke hemiplegic gait patterns. Normal gait and circumduction gait were performed at two gait speeds: 1.0 and 2.0 km/h. Each of the four gait conditions was performed in triplicate. According to previous studies, gait speeds among stroke patients, including those in the subacute and chronic phases, typically range from approximately 1.0 to 2.0 km/h [28–31]. Therefore, the gait speeds in this study were set to 1.0 and 2.0 km/h.

Circumduction gait is characterized by increased spatiotemporal asymmetry between the left and right limbs. Because of the difficulty in loading the paretic limb, the single-limb support time on the paretic side was approximately 60% of that on the non-paretic side, whereas the step length on the paretic side was approximately 120% of that on the non-paretic side. However, precisely controlling these spatiotemporal asymmetries and gait speeds in each trial is challenging. Therefore, to standardize the gait conditions as much

as possible, a gait pacing device was developed using two 5-meter-long LED tape strips, as shown in Figure 3. The intended foot contact positions were indicated by blue LEDs, which were changed to green LEDs at pre-programmed times to signal the next step. The participants walked between the two LED strips and placed their feet according to the right- and left-foot LEDs, thereby standardizing foot placement and timing. The timing of gait initiation was detected using a pressure sensor (SEN-09376, SparkFun), which triggered the start of LED guidance. Each trial began in a standing position, followed by a 5-meter walk, and ended again in a standing position. Because circumduction gait involves the paretic lower limb swinging outward in an arc, the participants were instructed to step such that the paretic foot moved along the LED path while drawing a lateral arc. Under these instructions, the paretic-side swing-phase foot trajectory showed increased lateral displacement (approximately 0.15–0.20 m) based on motion capture data, as shown in Figure 4. Additionally, during circumduction gait, the participants were instructed to flex the trunk laterally toward the paretic side and elevate the paretic-side pelvis during the swing phase to reduce the center of mass shifting toward the paretic limb.

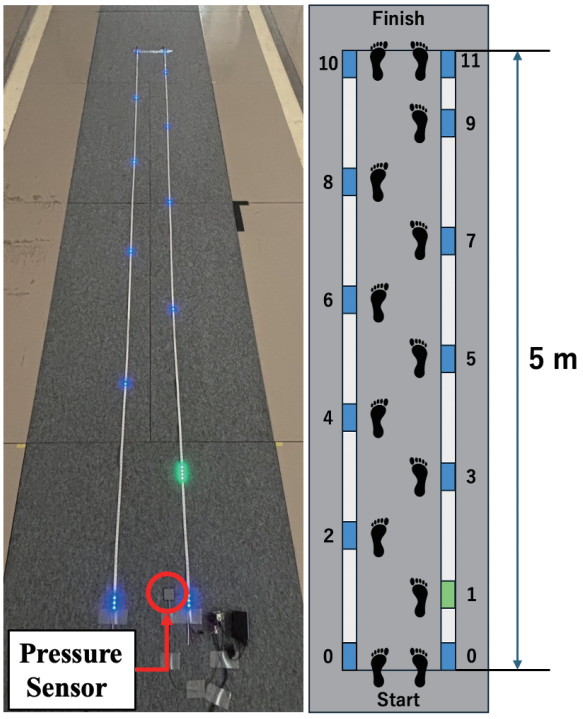

Figure 3. Custom-built gait pacing device.

5. Measurement Procedure

The posture-estimation device was mounted on the right knee joint. An appropriately sized knee supporter was selected to match the participant's leg circumference, and care was taken to ensure a secure fit without any looseness. During walking, three-axis acceleration and angular velocity were measured at a sampling frequency of 100 Hz using IMUs mounted on the thigh and shank. After each gait trial, the recorded data were wirelessly transmitted to a PC for analysis of gait events, such as foot contact timing and processing time of the Madgwick filter. Additionally, the resultant acceleration a_{total} was calculated using the 3-axis acceleration data (a_x, a_y, a_z) from the shank IMU, as shown in Equation (6). The timing of foot contact was defined as the moment when a_{total} exceeded the threshold of 1.5 G.

$$a_{total}=\sqrt{a_x^2+a_y^2+a_z^2} \quad (6)$$

Next, reflective markers were mounted on the participants' anatomical landmarks to perform gait measurements using the optical motion capture system, including the centers of rotation of the left and right hip joints, centers of rotation of the knee joints, lateral and medial malleoli, heads of the first and fifth metatarsals, and the heel. Three-dimensional gait motion was recorded at a sampling frequency of 120 Hz using a MAC3D System (Motion Analysis Corporation), which consisted of eight cameras. Posture and joint angles were calculated using KineAnalyzer (Kissei Comtec Co., Ltd.) motion

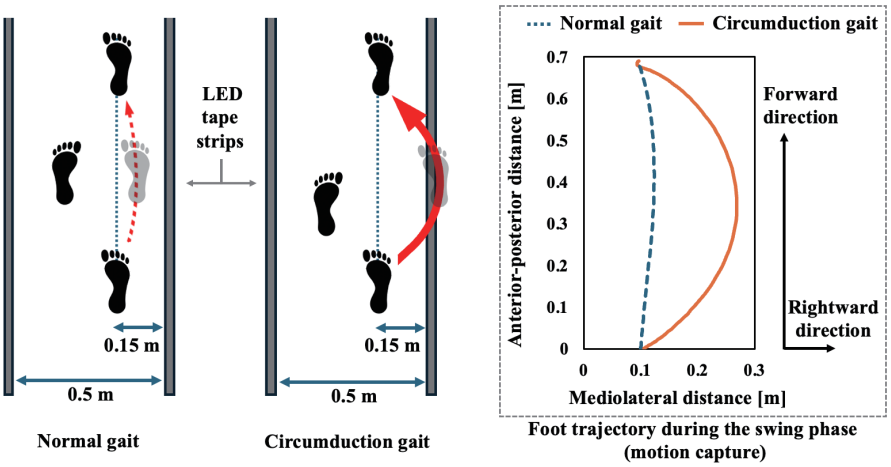

Figure 4. Kinematic definition of circumduction gait.

analysis software. The IMU and MAC3D measurements were performed simultaneously.

The participants were the authors themselves, consisting of two healthy adults without any motor or sensory impairments in the lower limbs. This study was conducted after confirming that it met the criteria for exemption from ethical review by Waseda University.

6. Analysis (Comparison Between Motion Capture MAC3D and IMU)

Assuming real-time posture estimation for FES control, the sampling of 3-axis acceleration and 3-axis angular velocity from two IMUs (sampling frequency: 100 Hz) and the output of FES control pulse signals (stimulation frequency: 20 Hz) were executed on a microcontroller. Posture estimation was then performed using pre-recorded acceleration and angular velocity data from each gait condition. The processing time was measured for each step. Although this analysis was conducted offline, if the sampling, posture estimation, and electrical stimulation control could be executed within 10 ms (corresponding to 100 Hz) on the microcontroller, the system could be considered capable of real-time processing. A sampling rate of at least 100 Hz is required for posture estimation under dynamic conditions [17]. Therefore, a processing time threshold of 10 ms was used as the benchmark because this is the maximum allowable time to maintain the 100 Hz sampling rate and real-time control of posture estimation and FES output.

The sampling rate of the MAC3D system was 120 Hz. To enable comparison with the IMU data, the posture and joint angle data obtained from MAC3D were resampled to 100 Hz using the statistical software R. To evaluate the accuracy of posture estimation using the Madgwick filter, the estimated posture was compared with the reference data obtained from motion capture. The accuracy was assessed using the root mean squared error (RMSE) and cross-correlation function. The cross-correlation function indicated the phase shift and the corresponding correlation coefficient (CC). As the start time of the IMU measurement was controlled via wireless communication, small temporal misalignments could occur. In such cases, the MAC3D data were time-shifted to synchronize with the IMU data. The RMSE represents the magnitude of error relative to the MAC3D data, whereas the CC indicates the similarity or degree of match between signals. For the analysis, three gait cycles from the middle portion of each 5 m gait trial were used.

Results

Table 2 lists the processing times required for sampling, posture estimation, and electrical stimulation control for each gait condition. No significant differences were observed between the conditions. The average processing time for IMU sampling was 0.68 ms, for the Madgwick filter 0.11 ms, and for electrical stimulation control 6.00 ms, resulting in a total average processing time of 6.80 ms. Thus, all processes were completed within the 10 ms threshold. An example of the Madgwick filter processing time is shown in Figure 5. The results were consistent regardless of gait type, and no delay exceeding 0.2 ms was observed. Table 3 lists the mean RMSE [°] and correlation coefficient (CC) for the thigh and shank inclination angles and knee joint angles for each gait. The RMSE values in parentheses, expressed as percentages, represent the ratio of the RMSE [°] to the total range of motion [°] measured by the motion capture system. Figure 6 shows an example of the waveforms obtained from posture estimation. The timing of foot contact on the IMU-mounted limb (right leg) was identified using the shank acceleration data and is indicated by the vertical dashed lines in the graph.

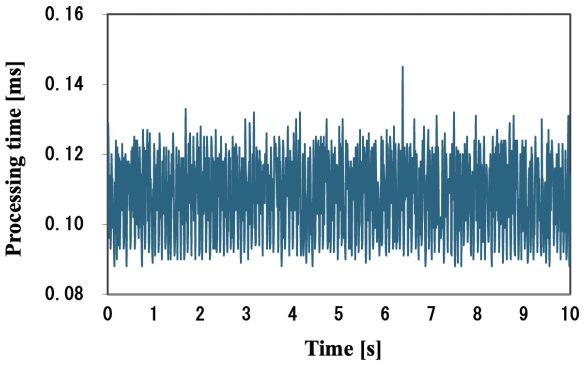

Figure 5. Example of processing time of the Madgwick filter (10 s).

Table 2. Mean and standard deviation of processing time for each gait.

	Sampling [μs]	Posture estimation [μs]	Stimulation [μs]	Total [μs]
Circumduction gait (slow)	683.3 ± 8.7	112.2 ± 12.5	6000.3 ± 22.4	6795.7
Circumduction gait (fast)	683.2 ± 8.4	112.3 ± 10.3	6000.2 ± 21.8	6795.7
Normal gait (slow)	683.3 ± 8.4	112.1 ± 11.5	6000.3 ± 25.2	6795.7
Normal gait (fast)	683.1 ± 8.5	111.9 ± 11.7	6000.2 ± 25.2	6795.3
Mean	683.2 ± 8.5	112.1 ± 11.5	6000.2 ± 23.7	6795.6

Table 3. Mean RMSE [°] and correlation coefficient (CC) during normal and circumduction gait.

		Sagittal plane			Frontal plane	
		Thigh inclination angle	Shank inclination angle	Knee joint angle	Thigh inclination angle	Shank inclination angle
Circumduction gait (slow)	RMSE [°]	2.288 (8%)	2.033 (5%)	2.858 (15%)	3.379 (17%)	3.271 (18%)
	CC	0.986	0.984	0.647	0.957	0.903
Circumduction gait (fast)	RMSE [°]	2.378 (6%)	2.122 (4%)	2.499 (10%)	2.837 (14%)	2.595 (13%)
	CC	0.992	0.992	0.924	0.945	0.940
Normal gait (slow)	RMSE [°]	1.543 (5%)	2.613 (5%)	3.280 (7%)	4.418 (61%)	5.175 (73%)
	CC	0.989	0.997	0.984	0.827	0.470
Normal gait (fast)	RMSE [°]	1.873 (5%)	3.607 (6%)	3.876 (9%)	4.717 (58%)	5.786 (66%)
	CC	0.990	0.994	0.973	0.828	0.657

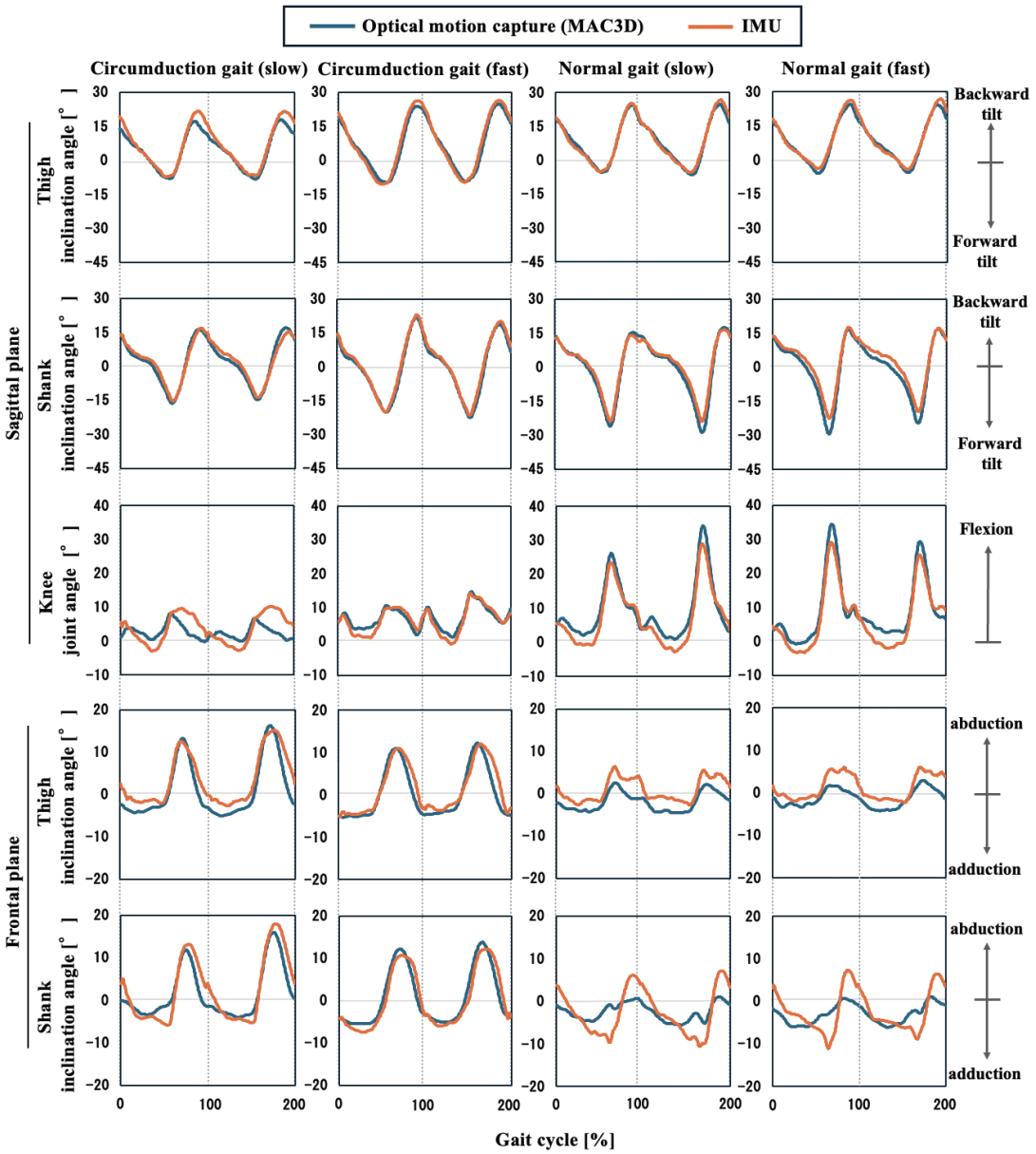

Figure 6. Example of posture angle waveforms during different gait conditions.

The RMSE values, indicating the error between the IMU and motion capture data, were within 4° for the sagittal plane posture angles and within 6° for all frontal plane posture angles. Additionally, the ratio of the RMSE to the range of motion was within 10% for all sagittal plane posture angles except for the knee joint angle during circumduction gait. The correlation coefficient (CC) was 0.97 or higher for nearly all sagittal plane posture angles, indicating high agreement. However, the CC values for the thigh and shank inclination angles in the frontal plane during normal gait were below 0.70, which was lower than those for the other posture angles.

When comparing the RMSE between circumduction and normal gait at the same gait speed, the values were all within 1°, however, only the sagittal plane thigh inclination angle was slightly higher during circumduction gait. The sagittal plane CC tended to be lower during circumduction gait, whereas the frontal plane CC was higher under the same conditions. As the lower limb swings outward during circumduction gait, the frontal plane thigh and shank inclination angles increase during the swing phase on the paretic side. As shown in the bottom left of Figure 6 (frontal plane posture angle waveform during circumduction gait), the proposed method successfully captured the circumduction motion. Conversely, as shown at the bottom right of Figure 6 (frontal plane posture angle waveform during normal gait), the frontal plane shank inclination angle during normal gait showed a maximum deviation of approximately 8° from the motion capture-based waveform.

Discussion

1. Madgwick Filter Processing Time

Sampling, posture estimation, and stimulation control could all be executed within 10 ms by measuring each processing time. The processing time of the nonlinear Kalman filter on a microcontroller has been reported to range from several milliseconds to several tens of milliseconds [32, 33], and one study reported that the Kalman filter required approximately 20 times more processing time than the Madgwick filter [34]. Therefore, employing a computationally efficient posture estimation method, such as that used in this study, utilizing posture information and incorporating additional processes, such as other sensor inputs or electromyography (EMG) measurements, becomes feasible, thereby enabling more accurate real-time FES control during abnormal gait.

2. Accuracy of Posture Estimation Using Madgwick Filter

The accuracy of the posture angle and joint angle estimation using the Madgwick filter was evaluated and compared with previous studies that employed similar measurements and gait conditions. In the study by Soussé et al. (2020), which estimated the sagittal plane knee joint angle during normal treadmill gait at 2 km/h using the Madgwick filter, the reported RMSE was 4.71°, and the CC was 0.96 [21]. In our study, posture estimation at a gait speed of 2 km/h resulted in an RMSE of 3.88° and CC of 0.97, indicating a higher level of accuracy than reported in the previous Madgwick filter-based study. In a study by Lora-Millán et al. (2021), which used an extended Kalman filter to estimate the sagittal plane knee joint angle during normal treadmill gait at an average speed of 2 km/h, the RMSE was 3.60° [35]. Although the RMSE in our study was slightly higher, the difference was within 0.3°, suggesting comparable estimation accuracy. In a study by Teruyama et al. (2013), which used a Kalman filter to estimate the sagittal plane thigh and shank inclination angles during normal treadmill gait at 1 km/h, the reported RMSEs were approximately 1.75° (CC: 0.99) for thigh inclination and 1.70° (CC: 0.99) for shank inclination [36]. In this study, the RMSEs at 1 km/h were 1.54° (CC: 0.99) for thigh inclination and 2.61° (CC: 0.99) for shank inclination, indicating higher estimation accuracy for the thigh inclination angle. However, the differences in the RMSEs were less than 1° in both cases, suggesting that the estimation accuracy for thigh and shank inclination angles was comparable to that of the previous study.

There is a lack of relevant literature regarding posture estimation during post-stroke hemiplegic gait and frontal plane thigh and shank inclination angles; thus, no direct comparison could be made with previous studies. However, compared with the sagittal plane posture angles, the estimation accuracy during circumduction gait was considered high, with errors within 1° (RMSE: less than 3.5°, CC: greater than 0.9). In a previous study that estimated the frontal plane inclination angle of the foot [24], the RMSE was reported to be 5.97°, which was more than 1° higher than that observed in the sagittal plane. Other studies [37−39] have also reported a trend of larger estimation errors in the frontal plane compared with the sagittal plane. This is likely due to the greater range of motion in the sagittal plane during gait, which increases the kinematic crosstalk in other planes.

In these previous studies, posture estimation was performed on a PC and was not designed for real-time processing. Moreover, owing to differences in gait conditions and measurement environments, direct comparisons are not straightforward. Nonetheless, the findings suggest that the estimation accuracy is comparable to that reported in previous studies.

3. Reproduced Hemiplegic Gait

In this study, a custom gait pacing device was developed to control spatiotemporal asymmetry and gait speed, thereby allowing healthy participants to

simulate the characteristic circumduction gait observed in individuals with hemiplegia. For overground gait, regulating gait speed using a metronome and pre-marked step intervals with tape is common [13]; however, this method is only applicable to symmetric normal gait. Conversely, the gait pacer developed in the present study allowed for the precise adjustment of temporal and spatial parameters, enabling a more accurate simulation of the hemiplegic gait, which is characterized by circumduction.

Next, the accuracy of posture angle estimation during simulated hemiplegic gait was examined and compared with that during normal gait. Although the error was within 1°, the estimation accuracy for the sagittal plane thigh inclination angles was lower during circumduction than during normal gait. This may be attributed to the greater rotational movement of the thigh during circumduction gait, which likely increases the influence of centripetal and tangential accelerations. Conversely, the estimation accuracy for the frontal plane inclination angles was high and remained stable even at higher gait speeds. Furthermore, as shown in the posture angle waveforms in Figure 6, the frontal plane inclination increased in the abduction direction during circumduction, with peaks reaching approximately 10−15°. These findings suggest the potential to evaluate circumduction movement and apply acceleration and angular velocity compensation based on the degree of circumduction or to establish appropriate thresholds when circumduction is detected, which may enhance FES control.

4. IMU Mounting Positions and Methods

The CC for the frontal plane shank inclination angle during normal gait was particularly low, and the waveform shown in Figure 6 indicates poor agreement with the MAC3D data. This is likely owing to the small range of motion in the frontal plane during normal gait, which makes the estimation more susceptible to errors. Additionally, other potential sources of IMU instability may have contributed to the decreased accuracy. These include misalignment between the body axis and IMU axis after mounting, as well as vibrations of the soft tissue [39, 40]. In this study, the IMUs were mounted on the lateral sides of the thigh and shank. However, because the mounting surfaces of the lower limbs are curved, the IMU orientation may not remain consistently fixed. Therefore, examining more stable IMU mounting positions to improve reliability is necessary.

Conclusion

Stroke patients with hemiplegia often walk in abnormal postures because of spasticity and muscle weakness, which differ significantly from those of healthy individuals. Functional electrical stimulation (FES) is used to support gait in individuals with hemiplegia, but accurate gait phase detection is essential for controlling the timing of stimulation. However, conventional gait phase detection methods developed for normal gait tend to show reduced accuracy when applied to abnormal gait. Therefore, developing a posture-based gait phase detection algorithm, where real-time posture estimation plays a critical role, is necessary. Moreover, lower-limb posture information can be utilized for post-discharge follow-up, gait analysis during daily life, orthosis selection, and adjustment of the support force. In this study, we implemented posture estimation in an FES device and evaluated the processing time when posture estimation was performed on a microcontroller using a computationally efficient Madgwick filter. Two healthy adults performed normal gait and gait reproducing the characteristic circumduction pattern of hemiplegic gait. The posture angles estimated using the IMUs were compared with reference data obtained from a motion capture system. As a result, the sagittal plane posture angles were estimated with an accuracy comparable to that reported in previous studies. In the frontal plane, the estimation accuracy was relatively high during circumduction gait but tended to be lower during normal gait. Additionally, the acceleration and angular velocity, posture estimation, and electrical stimulation control were all executed on the microcontroller within the required processing time of 10 ms (corresponding to 100 Hz real-time operation). These results demonstrate that real-time FES control is practically achievable without compromising estimation accuracy compared with previous studies.

Acknowledgments

This work was supported by JSPS KAKENHI (Grant Number JP23KJ2046). The authors declare no conflict of interest related to this study.

References

1. Ota M, Aoki J, Fuji C, Yamada T, Tamori M. Effects of Gait Training Using Functional Electrical Stimulation of the Tibialis Anterior Muscle on the Gait Pattern of Convalescent Hemiplegic Stroke Patients. Rigakuryoho Kagaku 2021; 36(1): 119−23. Japanese.
2. Jaqueline da Cunha M, Rech KD, Salazar AP, Pagnussat AS. Functional electrical stimulation of the peroneal nerve improves post-stroke gait speed when combined with physiotherapy. A systematic review and meta-analysis. Ann Phys Rehabil Med 2021; 64(1): 101388.
3. Marquez-Chin C, Popovic MR. Functional electrical stimulation therapy for restoration of motor function after spinal cord injury and stroke: a review. Biomed Eng Online 2020; 19(1): 34.
4. Hausdorff JM, Ring H. Effects of a new radio frequency-controlled neuroprosthesis on gait symmetry and rhythmicity in patients with chronic hemiparesis. Am J Phys Med Rehabil 2008; 87(1): 4−13.

5. Bethoux F, Rogers HL, Nolan KJ, Abrams GM, Annaswamy TM, Brandstater M, et al. The effects of peroneal nerve functional electrical stimulation versus ankle-foot orthosis in patients with chronic stroke: a randomized controlled trial. Neurorehabil Neural Repair 2014; 28(7): 688–97.
6. Prasanth H, Caban M, Keller U, Courtine G, Ijspeert A, Vallery H, von Zitzewitz J. Wearable Sensor-Based Real-Time Gait Detection: A Systematic Review. Sensors. 2021; 21(8): 2727.
7. Rueterbories J, Spaich EG, Larsen B, Andersen OK. Methods for gait event detection and analysis in ambulatory systems. Med Eng Phys. 2010; 32(6): 545–52.
8. Kotiadis D, Hermens HJ, Veltink PH. Inertial Gait Phase Detection for control of a drop foot stimulator Inertial sensing for gait phase detection. Med Eng Phys. 2010; 32(4): 287–97.
9. Mansfield A, Lyons GM. The use of accelerometry to detect heel contact events for use as a sensor in FES assisted walking. Med Eng Phys. 2003; 25(10): 879–85.
10. Picerno P. 25 years of lower limb joint kinematics by using inertial and magnetic sensors: A review of methodological approaches. Gait Posture 2017; 51: 239–46.
11. Tadano S, Takeda R, Miyagawa H. Three dimensional gait analysis using wearable acceleration and gyro sensors based on quaternion calculations. Sensors 2013; 13(7): 9321–43.
12. Cooper G, Sheret I, McMillan L, Siliverdis K, Sha N, Hodgins D, Kenney L, Howard D. Inertial sensor-based knee flexion/extension angle estimation. J Biomech 2009; 42(16): 2678–85.
13. Saito A, Miyawaki K, Kizawa S, Kobayashi Y. A study on estimating the knee joint angle during walking using the motion sensors (Focusing on the effect of centrifugal acceleration and tangential acceleration), Transactions of the JSME 2018; 84(857): 17–00488.
14. Sy LWF, Lovell NH, Redmond SJ. Estimating Lower Limb Kinematics Using a Lie Group Constrained Extended Kalman Filter with a Reduced Wearable IMU Count and Distance Measurements. Sensors 2020; 20(23): 6829.
15. Feldhege F, Mau-Moeller A, Lindner T, Hein A, Markschies A, Zettl UK, Bader R. Accuracy of a custom physical activity and knee angle measurement sensor system for patients with neuromuscular disorders and gait abnormalities. Sensors 2015; 15(5): 10734–52.
16. Mahony RE, Hamel T, Pflimlin JM. Nonlinear Complementary Filters on the Special Orthogonal Group. IEEE Transactions on Automatic Control 2008; 53(5): 1203–18.
17. Madgwick SO, Harrison AJ, Vaidyanathan R. Estimation of IMU and MARG orientation using a gradient descent algorithm. IEEE International Conference on Rehabilitation Robotics 2011, 1–7.
18. Feng K, Li J, Zhang X, Shen C, Bi Y, Zheng T, Liu J. A New Quaternion-Based Kalman Filter for Real-Time Attitude Estimation Using the Two-Step Geometrically-Intuitive Correction Algorithm. Sensors 2017; 17(9): 2146.
19. de Almeida TF, Morya E, Rodrigues AC, de Azevedo Dantas AFO. Development of a Low-Cost Open-Source Measurement System for Joint Angle Estimation. Sensors 2021; 21(19): 6477.
20. Fernandez IG, Ahmad SA, Wada C. Inertial Sensor-Based Instrumented Cane for Real-Time Walking Cane Kinematics Estimation. Sensors 2020; 20(17): 4675.
21. Soussé R, Verdú J, Jauregui R, Ferrer-Roca V, Balocco S. Non-rigid alignment pipeline applied to human gait signals acquired with optical motion capture systems and inertial sensors. J Biomech 2020; 98: 109429.
22. Bachmann ER, Xiaoping Yun, Peterson CW. An investigation of the effects of magnetic variations on inertial/magnetic orientation sensors. IEEE International Conference on Robotics and Automation, 2004. Proceedings. ICRA '04. 2004; 2(2): 1115–22.
23. de Vries WH, Veeger HE, Baten CT, van der Helm FC. Magnetic distortion in motion labs, implications for validating inertial magnetic sensors. Gait Posture 2009; 29(4): 535–41.
24. d'Andrea F, Taylor P, Yang K, Heller B. Can inertial measurement unit sensors evaluate foot kinematics in drop foot patients using functional electrical stimulation? Front Hum Neurosci 2023; 17: 1225086.
25. Niswander W, Wang W, Kontson K. Optimization of IMU Sensor Placement for the Measurement of Lower Limb Joint Kinematics. Sensors 2020; 20(21): 5993.
26. Fasel B, Spörri J, Schütz P, Lorenzetti S, Aminian K. Validation of functional calibration and strap-down joint drift correction for computing 3D joint angles of knee, hip, and trunk in alpine skiing. PLoS One 2017; 12(7): e0181446.
27. Favre J, Jolles BM, Aissaoui R, Aminian K. Ambulatory measurement of 3D knee joint angle. J Biomech 2008; 41(5): 1029–35.
28. Motoya R, Yamamoto S, Naoe M, Taniguchi R, Kawahara A, Iwata T. Classification of abnormal gait patterns of poststroke hemiplegic patients in principal component analysis. Jpn J Compr Rehabil Sci. 2022; 12: 70–7.
29. Bae YH, Ko YJ, Chang WH, Lee JH, Lee KB, Park YJ, Ha HG, Kim YH. Effects of Robot-assisted Gait Training Combined with Functional Electrical Stimulation on Recovery of Locomotor Mobility in Chronic Stroke Patients: A Randomized Controlled Trial. J Phys Ther Sci. 2014; 26(12): 1949–53.
30. Bethoux F, Rogers HL, Nolan KJ, Abrams GM, Annaswamy T, Brandstater M, Browne B, Burnfield JM, Feng W, Freed MJ, Geis C, Greenberg J, Gudesblatt M, Ikramuddin F, Jayaraman A, Kautz SA, Lutsep HL, Madhavan S, Meilahn J, Pease WS, Rao N, Seetharama S, Sethi P, Turk MA, Wallis RA, Kufta C. Long-Term Follow-up to a Randomized Controlled Trial Comparing Peroneal Nerve Functional Electrical Stimulation to an Ankle Foot Orthosis for Patients With Chronic Stroke. Neurorehabil Neural Repair. 2015; 29(10): 911–22.
31. Morone G, Fusco A, Di Capua P, Coiro P, Pratesi L.

Walking training with foot drop stimulator controlled by a tilt sensor to improve walking outcomes: a randomized controlled pilot study in patients with stroke in subacute phase. Stroke Res Treat. 2012; 2012: 523564.
32. Fico VM, Arribas CP, Soaje AR, Prats MÁ, Utrera SR, Vázquez AL, et al. Implementing the Unscented Kalman Filter on an embedded system: A lesson learnt. IEEE International Conference on Industrial Technology (ICIT) 2015; 2010−2014.
33. Valade A, Acco P, Grabolosa P, Fourniols JY. A Study about Kalman Filters Applied to Embedded Sensors. Sensors 2017; 17(12): 2810.
34. Caruso M, Sabatini AM, Laidig D, Seel T, Knaflitz M, Della Croce U, Cereatti A. Analysis of the Accuracy of Ten Algorithms for Orientation Estimation Using Inertial and Magnetic Sensing under Optimal Conditions: One Size Does Not Fit All. Sensors 2021; 21(7): 2543.
35. Lora-Millan JS, Hidalgo AF, Rocon E. An IMUs-Based Extended Kalman Filter to Estimate Gait Lower Limb Sagittal Kinematics for the Control of Wearable Robotic Devices. IEEE Access 2021; 9: 144540−144554.
36. Teruyama Y, Watanabe T. Effectiveness of variable-gain Kalman filter based on angle error calculated from acceleration signals in lower limb angle measurement with inertial sensors. Comput Math Methods Med 2013; 2013: 398042.
37. Palermo E, Rossi S, Patané F, Petrarca M, Castelli E, Cappa P. Experimental validation of a sensor to segment calibration procedure for MIMU based gait analysis. Gait & Posture 2013; 38: S110.
38. Han YC, Wong KI, Murray I. 2-Point Error Estimation Algorithm for 3-D Thigh and Shank Angles Estimation Using IMU. IEEE Sensors Journal 2018; 18: 8525−31.
39. Akbarshahi M, Schache AG, Fernandez JW, Baker R, Banks S, Pandy MG. Non-invasive assessment of soft-tissue artifact and its effect on knee joint kinematics during functional activity. J Biomech 2010; 43(7): 1292−301.
40. McGrath T, Stirling L. Body-Worn IMU-Based Human Hip and Knee Kinematics Estimation during Treadmill Walking. Sensors 2022; 22(7): 2544.